# Wavelet-transform-based damping identification of a super-tall building under strong wind loads

An Xu[*1,2,3,4], Jiurong Wu[1,2,3] and Ruohong Zhao[1,2,3]

[1]*Engineering Technology Research and Development Center for Structural Wind Resistance and Health Monitoring in Guangdong Province, Guangzhou University, Guangzhou, 510006, China*
[2]*Research Center for Structural Safety and Health Monitoring of Guangdong Education Department ,Guangzhou University, Guangzhou, 510006,China*
[3]*Guangzhou Municipal Key Laboratory for Structural Safety and Health Monitoring, Guangzhou University, Guangzhou, 510006, China*
[4]*Key Laboratory of Structure and Wind Tunnel of Guangdong Higher Education Institutes, Shantou 515063, China*

**Abstract.** A new method is proposed in this study for estimating the damping ratio of a super tall building under strong wind loads with short-time measured acceleration signals. This method incorporates two main steps. Firstly, the power spectral density of wind-induced acceleration response is obtained by the wavelet transform, then the dynamic characteristics including the natural frequency and damping ratio for the first vibration mode are estimated by a nonlinear regression analysis on the power spectral density. A numerical simulation illustrated that the damping ratios identified by the wavelet spectrum are superior in precision and stability to those values obtained from Welch's periodogram spectrum. To verify the efficiency of the proposed method, wind-induced acceleration responses of the Guangzhou West Tower (GZWT) measured in the field during Typhoon Usagi, which affected this building on September 22, 2013, were used. The damping ratios identified varied from 0.38% to 0.61% in direction 1 and from 0.22% to 0.59% in direction 2. This information is expected to be of considerable interest and practical use for engineers and researchers involved in the wind-resistant design of super-tall buildings.

**Keywords:** wind effect; tall building; field measurement; damping ratio

## 1. Introduction

In recent years, super-tall buildings have usually been constructed of light-weight, and high strength, materials and tend to be more flexible and lightly damped than those built in the past. Such buildings are thus sensitive to dynamic loads such as strong wind, which results in more emphasis on studies of wind effects on super-tall buildings than ever before (Li *et al*. 1998, Zhi *et al*. 2011, Fu *et al*. 2012). Natural frequencies and damping ratios are very important parameters affecting the dynamic response of structures, under wind load or earthquake excitation. The natural frequencies can be conveniently obtained from finite element analysis with reasonable accuracy.

---

∗Corresponding author, Associate Professor, E-mail: rocky-xu@qq.com

However, it is very difficult, or impossible, to estimate the structural damping ratio accurately prior to construction (Wu *et al.* 2007). It has been recognized that the most reliable evaluations of dynamic characteristics can be obtained from experimental measurements of a prototype building, and the identified damping ratios from field measured acceleration data of constructed building are helpful for determining damping ratios of super-tall buildings in their design process (Wu *et al.* 2007). In the past several years, field measurements of damping ratios were conducted for tall buildings throughout the world, and there had been many advances in the field of damping ratio identification (Wu *et al.* 2007, Li *et al.* 2006, 2003, Campbell *et al.* 2007), but overall, there is an obvious scarcity of damping data for super-tall buildings (building height > 300 m) under strong wind loads.

On the other hand, modal parameter identifications from ambient vibration data have received considerable attention in recent years. A variety of methods have been developed for extracting modal parameters from ambient vibration tests on structures (Mahdi *et al.* 2013, Le *et al.* 2013). In their studies, it was usually assumed that the input excitation behaves as a broadband stochastic process which can be modeled by stationary filtered white noise (Le *et al.* 2013). However, the wind load acting on a super-tall buildings during a typhoon passage is usually non-stationary due to the variation of wind speed and wind direction, and thus the response of the building due to wind excitation is also non-stationary during a typhoon's passage (Li *et al.* 1998, Zhi *et al.* 2011, Wu *et al.* 2007).

It is noteworthy that the wind speed during a typhoon passage of a super-tall building is not always large during the landing and decay of the storm. In fact, the wind-induced response with large amplitude level usually lasts for a very short period of time, for instance 20 or 30 minutes (Zhi *et al.* 2011, Fu *et al.* 2012, Wu *et al.* 2007). Actually, the implicit damping information during this short-time period is a really important parameter for estimating of the wind effects on structures during their design process. In this paper, a new approach was proposed for evaluating damping ratios of a super tall building under strong wind loads. The acceleration data with a large amplitude level during a short-time period were extracted from the original measured acceleration data for dynamic characteristic analysis, the power spectral density of the extracted data was then obtained by an approach based on the wavelet transform. Finally, both the natural frequency and the damping ratio for the first mode were identified by curve-fitting on the power spectral density in the region near the first natural frequency.

## 2. Methodology

Since the wind-induced response of a super-tall building may usually be dominated by its first vibration mode (Tschanz and Davenport 1983, Gu *et al.* 2011), only the wind-induced response contributed from the first vibration mode was considered in this study. The wind-induced response of a super-tall building can be obtained by modal superposition method with its transformed form into the dynamic equation with single-degree-of-freedom as

$$\ddot{q}(t) + 2\zeta_1\omega_1\dot{q}(t) + \omega_1^2 q(t) = F_1(t) \tag{1}$$

where $\omega_1$ and $\zeta_1$ are the undamped natural circular frequency and damping ratio for the first mode; $q(t)$ and $F_1(t)$ are the generalized modal coordinate (or displacement) and generalized modal force for the first vibration mode, respectively.

The Fourier spectral density of the generalized modal displacement can be evaluated as:

$$S_{qq}(f) = \frac{S_{F_1F_1}(f)}{\left(1 - \left(\frac{f}{f_1}\right)^2\right) + \left(2\zeta_1 \frac{f}{f_1}\right)^2} \tag{2}$$

where $S_{qq}(f)$ and $S_{F_1F_1}(f)$ are the power spectral densities of $q(t)$ and $F_1(t)$, respectively, and $f_1$ is the natural frequency for the first mode.

The wind induced response of a super tall building during a typhoon passage is usually non-stationary. With careful extracting the measured data during a short time with constant mean wind speed and constant wind direction, the acceleration samples extracted could be assumed to be stationary data. Therefore, the power spectral density of wind-induced acceleration could be expressed by the following equation

$$S_{\ddot{q}\ddot{q}}(f) = (2\pi f)^4 S_{qq}(f) = \frac{(2\pi f)^4 S_{F_1F_1}(f)}{\left(1 - \left(\frac{f}{f_1}\right)^2\right) + \left(2\zeta \frac{f}{f_1}\right)^2} \tag{3}$$

Many researches have indicated that the $\log_{10}(S_{F_1F_1}(f))$ decreases approximately linearly with the increase of $\log_{10}(f)$, when the frequency $f$ is located near the natural frequency for the first mode of the building (Fu *et al.* 2008, Liang *et al.* 2005, Solari 1985). Therefore, the $S_{F_1F_1}(f)$ can be approximately expressed by the following equation in the limited range near the first natural frequency of the building.

$$S_{F_1F_1}(f) = \eta \cdot f^\gamma \tag{4}$$

The parameters $\eta$ and $\gamma$ in the above equation are undetermined coefficients related with the acting wind loads. Substituting Eq. (4) into Eq. (3) we get

$$S_{\ddot{q}\ddot{q}}(f) = \frac{(2\pi f)^4 \cdot \eta f^\gamma}{\left(1 - \left(\frac{f}{f_1}\right)^2\right) + \left(2\zeta_1 \frac{f}{f_1}\right)^2} = \frac{(2\pi)^4 \eta \cdot f^{\gamma+4}}{\left(1 - \left(\frac{f}{f_1}\right)^2\right) + \left(2\zeta_1 \frac{f}{f_1}\right)^2} \tag{5}$$

Let $\alpha = (2\pi)^4 \eta$ and $\beta = \gamma + 4$, then Eq. (5) can be rewritten as

$$S_{\ddot{q}\ddot{q}}(f) = \frac{\alpha f^\beta}{\left(1 - \left(\frac{f}{f_1}\right)^2\right) + \left(2\zeta_1 \frac{f}{f_1}\right)^2} \tag{6}$$

If the power spectra density of extracted short-time acceleration data could be obtained with

adequate precision, the parameters including $f_1$, $\zeta_1$, $\alpha$, $\beta$ can therefore be evaluated by curve-fitting analysis method. So it is important to estimate the power spectrum of the exacted short-time acceleration data precisely.

The Power Spectral Density (PSD) is commonly used to express the energy distribution of a random data in frequency domain, various methods have been developed for its estimation including the Welch's averaged modified periodogram method, the Yule-Walker Autoregressive (AR) method *et al*. (Stoica *et al*. 1997). When PSD is estimated by Welch's method, the input signal is usually divided into several segments. With *nfft* samples in each segment during the Fast Fourier Transform (FFT) processing, the value of *nfft* must be as large as possible to obtain the adequate frequency resolution of the spectrum. On the other hand, the number of divided segments must be as large as possible to achieve a smooth spectrum by averaging the spectrum for each segment data. Therefore, the implementation of the Welch's periodogram method requires a large amount of sampled data to ensure the adequate content and resolution in the frequency domain for the processed signal. Thus it is not suitable for the short-time signal analysis. The AR methods assume that the signal can be modeled as the output of an AR filter driven by a white noise sequence. The model order must be first determined. If the model order is too small, the spectrum will be highly smoothed but with low frequency resolution. If it is too high, false peaks from an abundant amount of poles begin to appear. It is necessary to specify an appropriate order in the AR model for accurate spectrum estimation, otherwise significant errors will be produced during the spectral estimation (Neumaier *et al*. 2001).

To overcome the deficiency of the Welch's periodogram and AR method, a simple method based on the continuous wavelet transform is presented in this paper for the spectral estimation on the short-time signals. The structural damping ratio was obtained by curve-fitting with nonlinear regression according to Eq. (6). Relevant applications illustrate the efficiency of this method.

## 3. Spectral estimation based on wavelet transform

The definition of continuous wavelet transform refers to Appendix A in this paper. In order to estimate the spectral estimation of a given signal, the relationship between continuous wavelet coefficients and power spectrum must be firstly specified. Eq. (A-3) in Appendix shows that the continuous wavelet transform can be regarded as a band-pass filter which passes frequencies within the range defined by $\Psi(a\omega)$ and rejects frequencies outside that range. If the energy of $\Psi(a\omega)$ is concentrated near its center frequency, the continuous wavelet transform will represent the localized characteristics of the analyzed signal in the frequency domain.

According to the physical definition of power spectrum, the average power of a given signal $x(t)$ is defined as

$$\overline{x}^2 = \lim_{T \to \infty} \frac{1}{T} \int_{-T/2}^{T/2} |x(t)|^2 dt \tag{7}$$

where $T$ is the sampling time, and $|x(t)|^2$ is the instantaneous power of $x(t)$. The Plancherel theorem, a special case of the Parseval's theorem, states that

$$\bar{x}^2 = \lim_{T \to \infty} \frac{1}{T} \int_{-\infty}^{\infty} |X(f)|^2 df = \int_{-\infty}^{\infty} \lim_{T \to \infty} \frac{1}{T} |X(f)|^2 df = \int_{-\infty}^{\infty} S_{xx}(f) df \tag{8}$$

where $x(t)$ and $X(f)$ are a Fourier transform pair and $S_{xx}(f) = \dfrac{1}{T} \lim_{T \to \infty} |X(f)|^2$ denotes the power spectral density of $x(t)$. Based on the above analysis, it is shown by Eq. (A-3) in Appendix that the instantaneous power of the wavelet coefficient is

$$P(a,b) = |W(a,b)|^2 \tag{9}$$

Therefore, the average power of the wavelet coefficients can be expressed as

$$P(a) = E[|W(a,b)|^2] \tag{10}$$

where $E[\cdot]$ means the mathematical expectation of $(\cdot)$. For each specified value of the scale factor $a$, there is a corresponding stretched or compressed wavelet function related with the value of $a$. The bandwidth and the center frequency of the wavelet function are $1/a$ of those values for the mother wavelet function respectively, as shown in Eq. (11).

$$f_a = \frac{1}{a} f_c \tag{11a}$$

$$\Delta f_a = \frac{1}{a} \Delta f_\psi \tag{11b}$$

where $f_c$ and $\Delta f_\psi$ are the center frequency and bandwidth of the mother wavelet, and $f_a$ and $\Delta f_a$ are the center frequency and bandwidth of the wavelet function specified by the scale factor $a$.

If $\Delta f$ denotes the bandwidth of the wavelet function, we get the following equation:

$$P(a) = E[|W(a,b)|^2] = \int_{\Delta f} G_W(f) df \tag{12}$$

in which $G_W(f)$ denotes the power spectral density of the wavelet coefficients. As mentioned before, the wavelet transform can be regarded as a band-pass filter. If the scale factor $a$ is specified, the output of the wavelet transform contains only the frequency components in the range of $\Delta f$. If $G_W(f)$ remains constant as $G_W(f_a)$ when the frequency $f$ is located in the frequency range $\Delta f$, Eq. (12) can be approximately rewritten as (Bai *et al.* 2010)

$$E[|W(a,b)|^2] = \int_{\Delta f} G_W(f) df = G_W(f_a) \cdot \Delta f \tag{13}$$

Therefore, the power spectral density of the wavelet coefficients can be expressed as the following equation:

$$G_W(f_a) = \frac{1}{\Delta f} E[|W(a,b)|^2] \tag{14}$$

According to the definition of wavelet transform, the wavelet coefficients can be regarded as the output of the original signal by wavelet transform. Therefore the power spectral density of the original signal $f(t)$ can be expressed as (Bai *et al*. 2010)

$$G_x(f_a) = \frac{1}{|H(f_a)|^2} G_W(f_a) \tag{15}$$

where $H(\cdot)$ denotes the transfer function. Eq. (15) expresses the relationship between the input and output of a linear time-invariant system in frequency domain with zero-initial conditions and zero-point equilibrium. Eq. (15) illustrates that the transfer function must be determined to evaluate the power spectral density of the input signal.

The transfer function is the Fourier transform of the impulse response function (IRF) of a dynamic system, as shown in Eq. (16)

$$H(f) = \int_{-\infty}^{\infty} h(t) e^{-i2\pi ft} dt \tag{16}$$

in which $h(t)$ denotes the impulse response function. Let $x(t)$ be the input of a linear dynamic system, the output $y(t)$ can be expressed as the convolution of $x(t)$ and the IRF $h(t)$, as shown in Eq. (17)

$$y(t) = x(t) * h(t) = \int_{-\infty}^{\infty} x(u) h^*(t-u) du \tag{17}$$

Comparing Eq. (A-2) with (17), it can be found that the transfer function of the wavelet transform can be expressed as (Bai *et al*. 2010)

$$H(f) = \sqrt{a} \Psi(a 2\pi f) e^{-i2\pi fb} \tag{18}$$

Hence, we obtain,

$$|H(f)|^2 = a |\Psi(a 2\pi f)|^2 \tag{19}$$

In this study, the complex Morlet wavelet function was selected as the mother wavelet function. It is expressed as

$$\psi(t) = \frac{1}{\sqrt{\pi f_b}} e^{i2\pi f_c t} e^{-\frac{t^2}{f_b}} \tag{20}$$

where $f_c$ and $f_b$ are the center frequency and bandwidth parameter, respectively. The bandwidth parameter $f_b$ controls the shape of the basic wavelet. The Fourier transform of the complex Morlet wavelet can be expressed as

$$\Psi(f) = e^{\pi^2 f_b (f - f_c)^2} \tag{21}$$

Thus the transfer function for the wavelet transform can be obtained by substituting Eq. (21) into Eq. (19). Now, Eq. (15) can be employed to evaluate the power spectrum of a given signal based on the wavelet transform.

## 4. Simulation

A numerical simulation was conducted to demonstrate the effectiveness of the proposed method in this study. Firstly the power spectral density of a simulated acceleration signal is defined in the form of Eq. (6), and three specified sets of parameters in the equation, as shown in Table 1.

Once the power spectrum of an acceleration signal is given, the times series of the signal can be simulated by the series superposition method in the following form

$$
\begin{aligned}
a(t) &= \sum_{n=1}^{N} \sqrt{2S(f)\Delta f} \, \cos(2\pi ft + \phi_n) \\
&= \sum_{n=1}^{N} \sqrt{2S(f)\Delta f} \, (\cos 2\pi ft \cos \phi_n - \sin 2\pi ft \sin \phi_n) \\
&= \sum_{n=1}^{N} \sqrt{2S(f)\Delta f} \, [\frac{1}{2}(\cos \phi_n - \frac{\sin \phi_n}{i})e^{i2\pi ft} + \frac{1}{2}(\cos \phi_n + \frac{\sin \phi_n}{i})e^{-i2\pi ft}]
\end{aligned}
\tag{22}
$$

where $f$, $t$ denotes frequency and time, respectively, $S(f)$ is the simulated power spectral density which is specified by 3 sets of parameters illustrated in Table 1, $\Delta f$ is the frequency interval, $\phi_n$ is the random phase angle which distributes uniformly in the interval of $[0, 2\pi]$, and $a(t)$ is the time series of simulated acceleration.

It should be clarified that the power spectrum of the simulated signal may not fit with the target spectrum very well on the basis of one simulation process. The simulation quality can be achieved through averaging with more simulation times. Fig. 1 showed the comparison of the averaged spectrum through 100 simulation tests with the target spectrum. It is seen that the spectrum of simulated signal is in good agreement with the target spectrum, which demonstrated the validity of the simulation method shown in Eq. (22).

The sampling frequency was set to be 25 Hz for all test cases. The sampling lengths for the three cases were set to be 16384, 32768 and 65536 to investigate the effect of the sampling length on the accuracy of the dynamic characteristics parameter identification. The power spectra of the simulation signals were estimated by two methods: the continuous-wavelet-transform-based method as described in Eq. (15) (CWT) and the most commonly used Welch's Averaged Modified Periodogram method (WAMPS). The selected Morlet wavelet parameters were set as $f_b = 4$ and $f_c = 2$ to ensure the frequency resolution. After obtaining the power spectral density by the above two methods, the parameters including $f_1$, $\zeta_1$, $\alpha$, $\beta$ in Eq. (6) can be estimated by non-linear curve-fitting in least-square sense.

The identified results for modal parameters for the simulated signals are shown in Table 2. It is

seen that the estimated results for natural frequency from the two methods are in good agreement with the target value. As the customized natural frequency was 0.19 Hz and the identified natural frequencies varied from 0.189 to 0.191 Hz, giving a maximum relative error for estimated results of about 5%. However, the identification accuracy of damping ratios by WAMPS method dropped significantly when the sampling length decreased from 65536 to 16384. However, the identification accuracies by the CWT method are maintained at a relatively high level, regardless of different sampling lengths. When different sampling lengths were selected from 65536 to 16384, the relative errors of identified damping ratios were 10%, 30% and 40% for the WAMPS method. The corresponding values for CWT dropped to 10%, 10% and 20% respectively. The effect of sampling lengths on the estimated accuracy by WAMPS method was clearly demonstrated through this example, especially for the identified damping ratios. However, the continuous wavelet transform can express the signal characteristic in both time and frequency domain, with different resolution scales. Therefore it is suitable to identify the dynamic characteristics in frequency domain for short-time signals. In order to reduce the unfavorable edge effects of CWT, the sampling length should not be too short. The minimum sampling length for CWT was 16384 in this study.

It should be noted that the damping ratio was always overestimated by both the CWT and the WAMPS methods; the reason might be that the estimated spectra by both methods have limited frequency resolutions, and could not reproduce all the features in the frequency domain for the target spectrum. The shape of estimated spectrum was then not such sharp as that of the target spectrum, leading to an overestimation of the damping ratio.

Since the identification of damping ratio is much more difficult than other dynamic parameters such as natural frequencies or mode shapes, relative error within 20% might be acceptable for practical applications. Therefore the proposed method might be regarded as a valid approach for damping ratio identification for short-time wind-induced vibration signals.
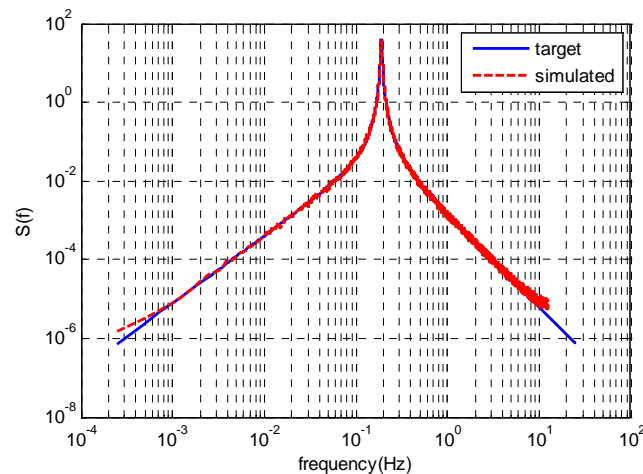


Fig. 1 Comparison of the target spectrum and spectrum of simulated signal

Table 1 Customization of parameters in Eq. (6) for simulation

| Case number | $\alpha$ | $\beta$ | $f_1$ (Hz) | $\zeta$ |
|---|---|---|---|---|
| 1 | 1 | 1.7 | 0.19 | 0.01 |
| 2 | 1 | 1.7 | 0.19 | 0.02 |
| 3 | 1 | 1.7 | 0.19 | 0.03 |

Table 2 Results of modal parameter identification of simulation data

| Case number | Identified modal parameters | Sampling length | | | | | |
|---|---|---|---|---|---|---|---|
| | | 65536 | | 32768 | | 16384 | |
| | | Wavelet spectrum | Modified periodogram spectrum | Wavelet spectrum | Modified periodogram spectrum | Wavelet spectrum | Modified periodogram spectrum |
| 1 | $f_1$ | 0.190 | 0.190 | 0.190 | 0.191 | 0.191 | 0.191 |
| | $\zeta_1$ | 0.011 | 0.011 | 0.011 | 0.014 | 0.012 | 0.013 |
| 2 | $f_1$ | 0.190 | 0.190 | 0.190 | 0.190 | 0.189 | 0.189 |
| | $\zeta_1$ | 0.021 | 0.022 | 0.022 | 0.022 | 0.021 | 0.024 |
| 3 | $f_1$ | 0.190 | 0.190 | 0.190 | 0.191 | 0.191 | 0.191 |
| | $\zeta_1$ | 0.032 | 0.033 | 0.034 | 0.036 | 0.033 | 0.036 |

## 5. Application and discussion

In order to validate the effectiveness of the proposed method for damping ratio identification for super-tall building under strong wind loads, field measurements of wind characteristics and wind-induced acceleration on the Guangzhou West Tower were conducted when Typhoon Usagi affected this tall building on September 22, 2013. The measured acceleration data were used to identify the damping ratio for the first mode of the building.

The Guangzhou West Tower (GZWT, now called "Guangzhou International Finance Centre" after its completion in 2010), which is 432 m high with 103 stories, is located in Guangzhou and was the tallest building in South China after its construction. The GZWT was designed and constructed with an innovative structural style which comprised a reinforced concrete core in conjunction with the perimeter concrete-filled steel tube (CFT) to provide its overall stiffness and stability. It was difficult to determine the damping ratio value in wind-induced vibration analysis during the design stage for such a new kind of building, therefore it is necessary to accumulate vibration data under strong wind actions and identify its damping ratio for the purpose of verifying the adopted damping ratio value in its design stage, and providing a reference for the damping ratios of other similar buildings.

A wind- and structural-monitoring system was installed at the GZWT to monitor its wind-induced response and wind characteristic around the building. Two ultra-low frequency

accelerometers were placed orthogonally along the two main axes on the 102th floor of the building, to record the acceleration of the building during the   passage of the typhoon, as shown in Fig. 2. Also, a propeller anemometer (R. M. Young Model 05106) and a 3D ultrasonic anemometer were installed on the mast erected above the roof of the building, as shown in Fig. 3.

Typhoon Usagi (international designation: 1319) was one of the most intense tropical cyclone in the northwest Pacific Ocean in 2013. Developing into a tropical storm to the east of the Philippines late on September 16, Usagi began explosive intensification on September 19, and ultimately became a violent and large typhoon. Afterwards, the system weakened slowly, crossed the Bashi Channel on September 21, and it made landfall over Guangdong, China on September 22. The moving path of Typhoon Usagi is shown in Fig. 4. During the GZWT was affected by Typhoon Usagi (from 22:00 on September 22 to 20:00 on September 23, 2013), data including wind speed, wind direction and wind-induced acceleration were recorded by the monitoring system for about 20 hours.
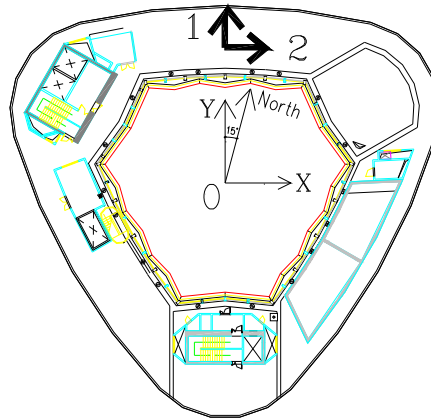


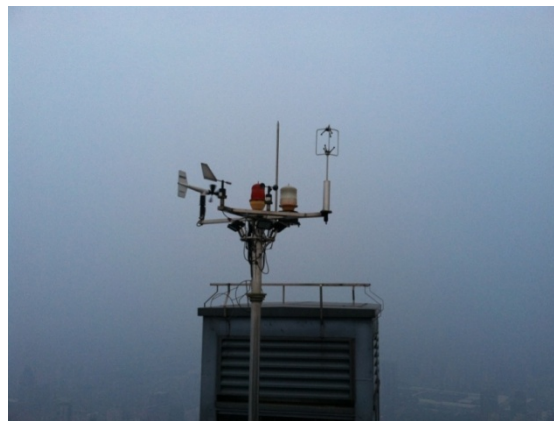Fig. 2 The installed accelerometer along two main-axis of the GZWT
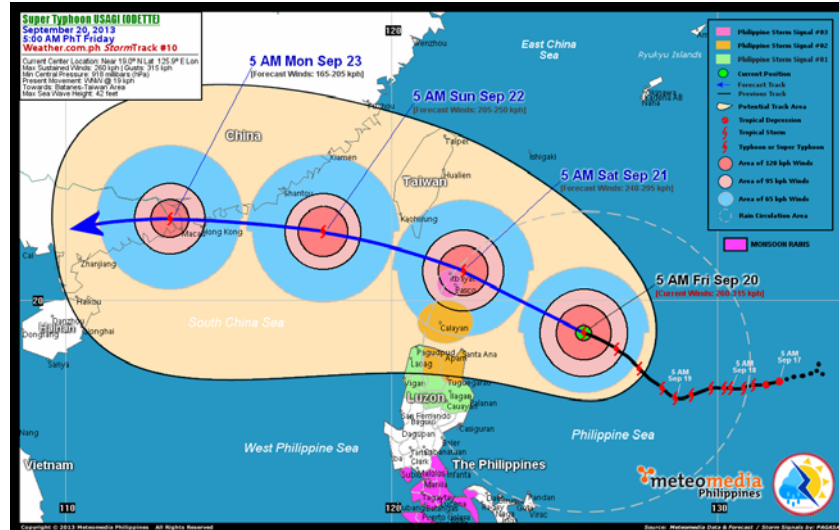


Fig. 3 The installed 2D and 3D anemometers

Fig. 4 Moving path of Typhoon Usagi

### 5.1 wind speed and wind direction

Data on wind speed and wind direction were recorded by a 2D propeller anemometer and a 3D ultrasonic anemometer. For the 2D propeller anemometer, the measured data were wind speed and wind direction in the horizontal plane. For the 3D ultrasonic anemometer, recorded data included the wind speed $u(i)$, azimuth angle $\gamma(i)$ and elevation angle $\beta(i)$. The results of horizontal wind speed and wind direction from the 2D propeller and 3D ultrasonic anemometer were in good agreement with each other. Here only results obtained from the 2D anemometer are presented for the sake of brevity. Acceleration data were measured by two accelerometers simultaneously with the sampling frequency of 25.6 Hz. The wind speed maintained a relatively large value for about five hours; the mean horizontal wind speed was 18.47 m/s and the corresponding horizontal wind direction varied slightly around 320°. The measured wind speed, wind direction and acceleration during the five hours are shown in Figs. 5 and 6, respectively.

According to the simulated results described in the previous section, 32768 samples from the recorded acceleration data were selected to analyze the natural frequency and damping ratio. The selected data along two main axes were shown in Figs. 6(a) and 6(b), and their measured and fitted wavelet spectrums are shown in Figs. 7(a) and 7(b) respectively. According to the fitted curve, the natural frequencies for the first mode in direction 1 and 2 are 0.1460 Hz and 0.1457 Hz, and the corresponding damping ratios in two directions are 0.41% and 0.36%, respectively.

An amplitude-dependent damping ratio model for super-tall buildings has been proposed by some researchers from field measured data (Wu *et. al*, 2007); the relationship between the structural damping ratio and the vibration amplitude was also studied in that paper. Some researchers selected the displacement as a description of vibration amplitude in damping estimation (Wu *et al*. 2007, Fu *et al*. 2012), However the displacement is not easy to obtain from

the measured acceleration data. Thus the root mean square (RMS) value of the acceleration data is chosen as an indicator of the structural vibration amplitude in this paper. The measured acceleration data were divided into many short-time segments; for each segment the measured acceleration was regarded as stationary with the assumption that the RMS value remained constant during this time duration. The variation of the identified damping ratios with their RMS accelerations are illustrated in Figs. 8(a) and 8(b). It shows that when the RMS acceleration was less than 2.0 mm/s$^2$, the damping ratios vary randomly from about 0.2% to 0.9%, which might mean that this method cannot produce stable identification results from vibration signals with a low amplitude level. The reason may be inadequate sign-noise-ratio existed in the recorded signals with low vibration amplitude, which reduced the accuracy of damping ratio identification results. However, the identified damping ratios were much more stable when the vibration amplitudes were greater than 0.2 mm/s$^2$. The identified damping ratios varied from 0.38% to 0.61% in direction 1, and 0.22% to 0.59% in direction 2 within a relatively narrow range.
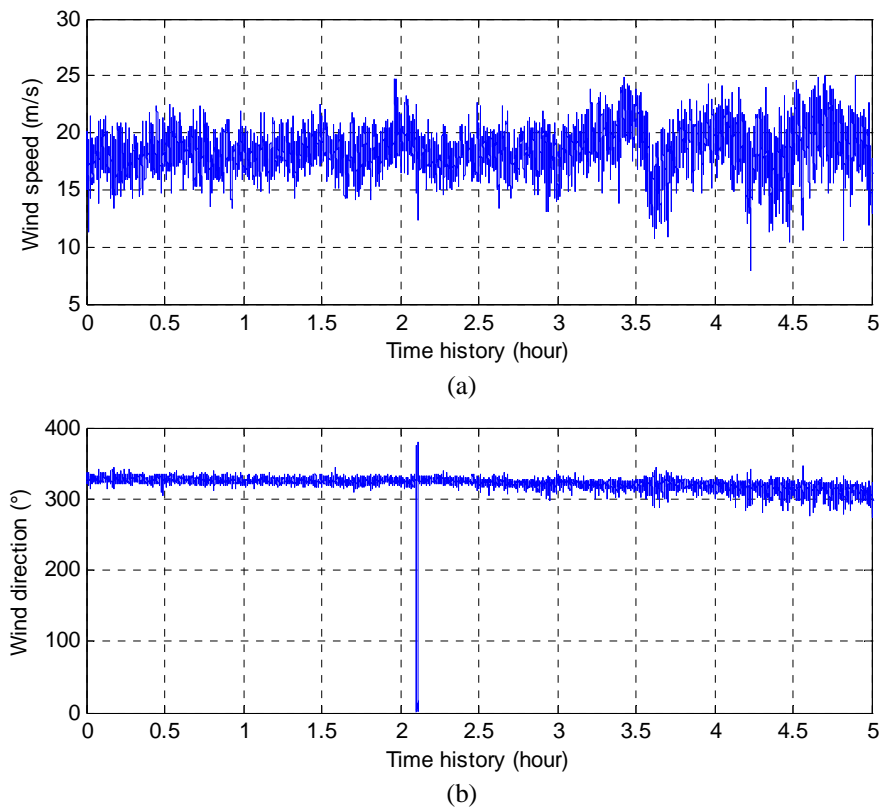


(a)

(b)

Fig. 5 (a) Time history of wind speed measured by 2D propeller anemometer and (b) Time history of wind direction measured by 2D propeller anemometer
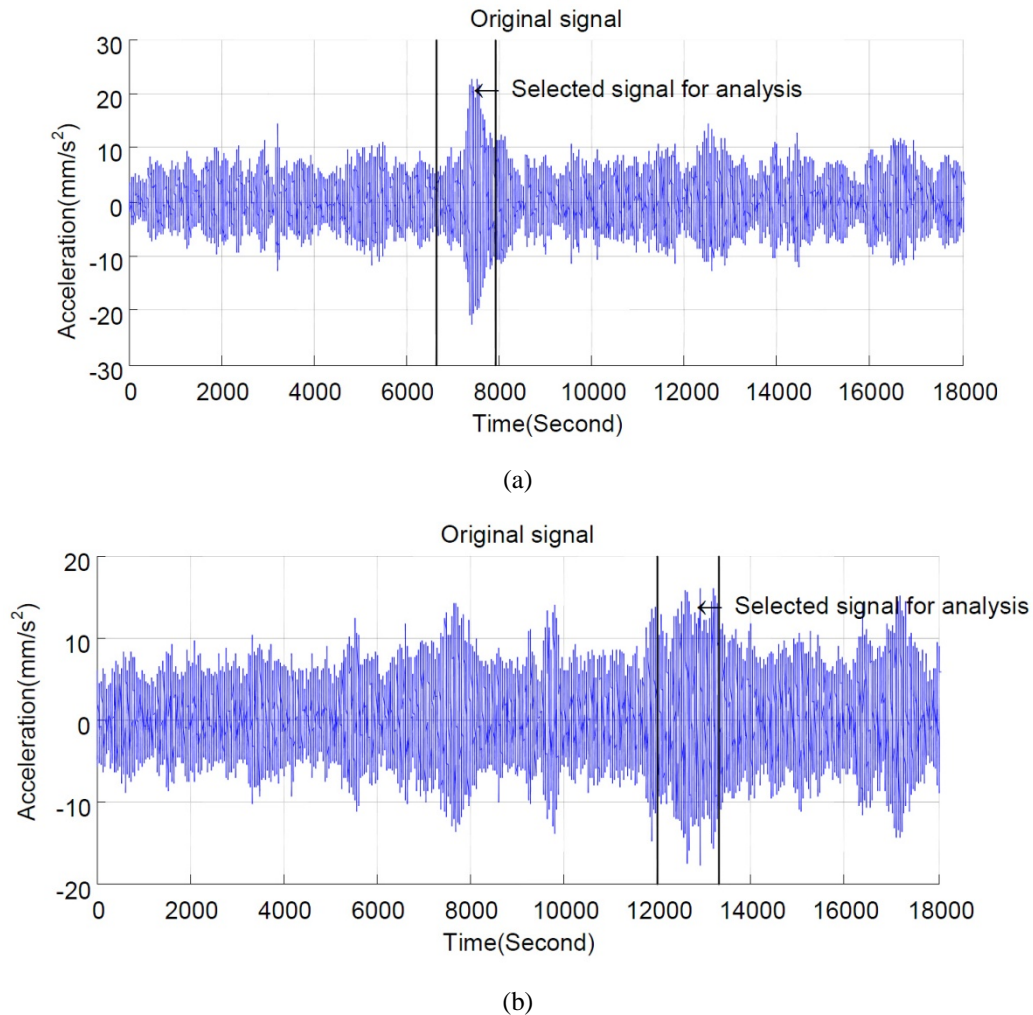
(a)



(b)

Fig. 6 (a) Selected data from acceleration response in Direction 1 and (b) Selected data from acceleration response in Direction 2

Other researchers had measured the wind-induced acceleration response of GZWT when Typhoon Megi affected this building on October 22, 2010 (Fu *et al.* 2012). It was reported from their studies that the identified damping ratios increased nonlinearly with the increase of the vibration amplitude. They varied from 0.24~0.36% in direction 1 and 0.20~0.35% in direction 2. Compared with the results of Fu *et al.*, the identified damping ratios of the GZWT seems to have no direct relationship with the structural vibration amplitude in this study. Even though in the Fu *et al.* study, some of the identified damping ratios were distributed discretely beside the fitted curve, and a non-linear relationship between damping ratios and the structural vibration amplitude was not very clear. For a steel-concrete composite structure such as GZWT, a constant of damping value of 1% is widely adopted for wind-induced human comfortability threshold check, and a

*An Xu, Jiurong Wu and Ruohong Zhao*

damping ratio of 3% is normally selected for the ultimate limit state design according to current many design codes and specifications; however, the identified damping ratios for the GZWT in this study are based on the measured data with low serviceability amplitudes. It is therefore desirable to accumulate more field measured data, under strong wind actions, to further the understanding of damping ratios of super-tall buildings.
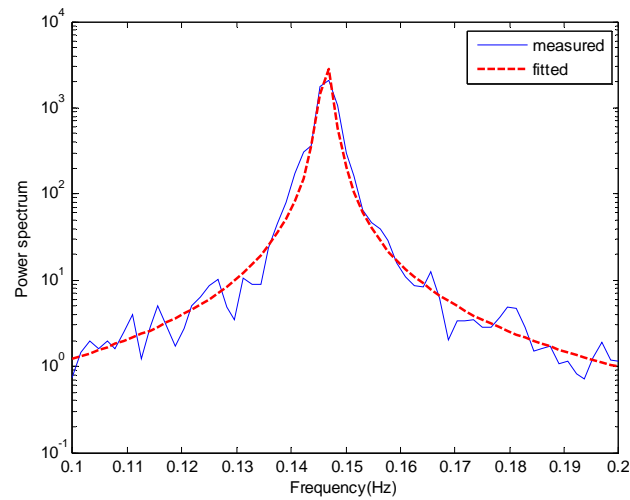


(a)
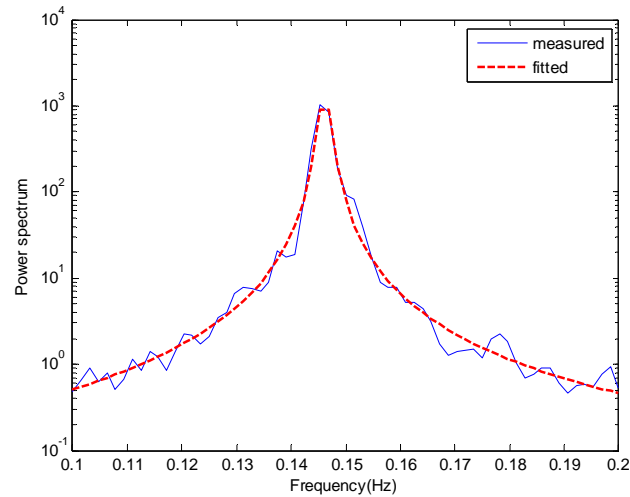


(b)

Fig. 7 (a) Measured and fitted wavelet spectrum of the selected data in Direction 1 and (b) Measured and fitted wavelet spectrum of the selected data in Direction 2
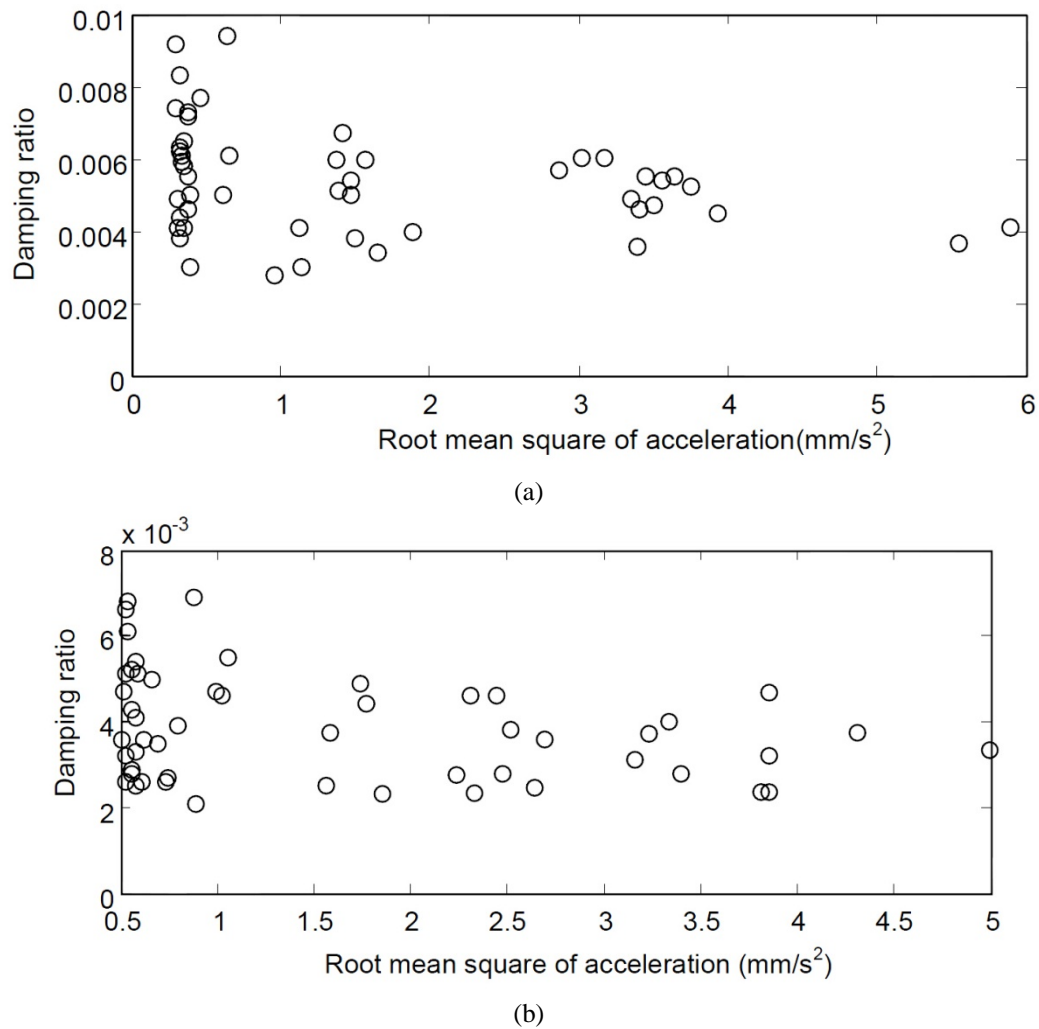
(a)



(b)

Fig. 8 (a) Relationship between the identified damping ratio and the root- mean-square acceleration in Direction 1 and (b) Relationship between the identified damping ratio and the root- mean-square acceleration in Direction 2

## 5. Conclusions

In this study, a new method is proposed for estimation of the damping ratios of super-tall buildings under wind loads, with short-time recorded acceleration data. This method contains two main steps including: (1) estimating the power spectral density of the short-time signal by the continuous wavelet transform, and (2) identify the dynamic characteristics including the natural frequency and damping ratio for the first mode by curve-fitting analysis on the estimated power spectral density by the CWT.

The results from numerical simulation data illustrate that the damping ratios identified from CWT are superior to those estimated values from the Welch's periodogram spectrum, in both precision and stability.   Higher frequency resolution for estimated power spectrum are obtained from the CWT method by adjusting the scaling factor during wavelet transform, and this method could provide more data points for curve-fitting than the Welch's averaged modified periodogram. Thus, it enabled more precise results from CWT method to be obtained.

The proposed method was further employed to estimate the natural frequencies and damping ratios for the first mode of a practical super tall building under the effect of typhoon. The identified damping ratios varied from about 0.38% to 0.61% in direction 1 and from about 0.22% to 0.59% in direction 2, and no obvious relationship seems to exist between the identified damping ratios and the vibration amplitudes. More field-measured data should be collected and analyzed, in order to further the understanding of damping characteristics in super tall buildings subjected to strong wind loads.


## Acknowledgements

## References

Bai, Q., Bao, W.B. and Jin, S.J. (2010), "Estimation of time-dependent power spectral density of seismic wave based on wavelet transform", *J. Shenyang Univ. Technol.*, **32**(3), 342-348 (in Chinese).

Campbell, S. , Kwok, K.C.S., Hitchcock, P.A., Tse, K.T. and Leung, H.Y. (2007), "Field measurements of natural periods of vibration and structural damping of wind-excited tall residential buildings", *Wind Struct.*, **10**(5), 401-420.

Fu, J.Y., Wu, J.R. and Xu, A. (2012), "Full-scale measurements of wind effects on Guangzhou West Tower", *Eng. Struct.*, **35**(1), 120-139.

Fu, J.Y., Li, Q.S. and Wu, J.R. (2008), "Spectral characteristics and correlation of dynamic wind forces on a super-tall building", *Struct. Des. Tall Spec.*, **17**, 471-489.

Gu, M. and Quan, Y. (2011), "Across-wind loads and effects of super-tall buildings and structures", *Sci. China*, **54**, 2531–2541.

Gu, M. (2009), "Study on wind loads and responses of tall buildings and structures", *Asia-Pac. Conf. Wind Eng.*, APCWE-VII

Le, T. and Patrick, P. (2013), "Modal identification based on the time-frequency domain decomposition of unknown-input dynamic tests", *Int. J. Mech Sci.*, **71**, 41-50.

Li, Q.S., Fu, J.Y., Xiao, Y.Q., Li, Z.N., Ni, Z.H., Xie, Z.N. and Gu, M. (2006), "Wind tunnel and full-scale study of wind effects on China's tallest building", *Eng. Struct.*, **28**, 1745-1758.

Li, Q.S., Yang, K., Wong, C.K. and Jeary, A.P. (2003), "The effect of amplitude-dependent damping on wind-induced vibrations of a super tall building", *J. Wind Eng. Ind. Aerod.*, **91**(9), 1175-1198.

Li, Q.S., Fang, J.Q., Jeary, A.P. and Wong, C.K. (1998), "Full scale measurements of wind effects on tall buildings", *J. Wind Eng. Ind. Aerod.*, **74-76**, 741-750.

Liang, S.Q., Li, Q.S., Zou, L.H. and Wu, J.R. (2005), "Simplified formulas for evaluation of across-wind dynamic responses of rectangular tall buildings", *Wind Struct.*, **8**(3), 197-212.

Mohammad Mahdi, A. and Mahmood, Y. (2013), "Estimation of damping ratio of TV towers based on ambient vibration monitoring", *Struct. Des. Tall Spec.*, **22**(11), 862-875.

Neumaier, A. and Schneider, T. (2001), "Estimation of parameters and eigenmodes of multivariate autoregressive models", *ACM Trans on Math Soft.*, **27**(1), 27-57.

Solari, G. (1985), "Mathematical model to predict 3-D wind loading on buildings", *J. Eng. Mech.* - ASCE 111(2), 254-275.

Spanos, P.D, (2004), "Evolutionary spectra estimation using wavelets", *J. Eng. Mech. - ASCE*, **130**(8),952-960.

Stoica, P. and Moses R.L. (1997), *Introduction to Spectral Analysis*, Prentice-Hall.

Tschanz, T. and Davenport, A.G. (1983), "The base balance technique for the determination of dynamic wind loads", *J. Wind Eng. Ind. Aerod.*, **13**, 429-439.

Wu, J.R., Liu, P.F. and Li, Q.S., (2007), "Effects of amplitude-dependent damping and time constant on wind-induced responses of super tall building", *Compu. Struct.*, **85**, 1165-1176

Zhi, L.H., Li, Q.S., Wu, J.R. and Li, Z.N. (2011), "Field monitoring of wind effects on a super-tall building during typhoons", *Wind Struct.*, **14**(3), 253-283.

*JH*

## Appendix A:   Definition of continuous wavelet transform

Consider a function $f(t)$ with finite energy , that is

$$\int_{-\infty}^{\infty} \left| f(t) \right|^2 dt < \infty \tag{A-1}$$

The continuous wavelet transform of $f(t)$ is defined as (Spanos *et al*. 2004)

$$W(a,b) = \frac{1}{\sqrt{a}} \int_{-\infty}^{\infty} f(t)\psi^* \left( \frac{t-b}{a} \right) dt \tag{A-2}$$

where $\psi(t)$, $a$, $b$ are the so-called mother wavelet, the scale parameter and the time parameter, respectively, and $W(a,b)$ is the continuous wavelet coefficient. The symbol (*) denotes complex conjunction.

Eq. (A-2) can be rewritten in frequency domain as:

$$W(a,b) = \frac{\sqrt{a}}{2\pi} \int_{-\infty}^{\infty} F(\omega)\Psi(a\omega)e^{j\omega b} d\omega \tag{A-3}$$

in which $F(\omega)$, $\Psi(\omega)$ are the Fourier transform of $f(t)$ and $\psi(t)$, respectively.